Title

Measuring Metal–Metal Communication in a Series of Ketimide-Bridged [Fe2]6+ Complexes

Journal

Inorganic Chemistry, 62(30)

ISSN

0020-1669

Authors

Hertler, Phoebe R
Lewis, Richard A
Wu, Guang
et al.

Publication Date

2023-07-31

DOI

10.1021/acs.inorgchem.3c01109

Measuring Metal–Metal Communication in a Series of Ketimide-bridged $[Fe_2]^{6+}$ Complexes

Phoebe R. Hertler, Richard A. Lewis, Guang Wu, and Trevor W. Hayton*

Department of Chemistry and Biochemistry, University of California Santa Barbara, Santa Barbara, CA 93106

ABSTRACT: Reaction of $Fe(acac)_3$ with 3 equiv of $Li(N{=}C(R)Ph)$ (R = Ph, ^{t}Bu) results in formation of the $[Fe_2]^{6+}$ complexes, $[Fe_2(\mu\text{-}N{=}C(R)Ph)_2(N{=}C(R)Ph)_4]$ (R = Ph, **1**; ^{t}Bu, **2**), in low to moderate yields. Reaction of $FeCl_2$ with 6 equiv of $Li(N{=}C_{13}H_8)$ ($HN{=}C_{13}H_8$ = 9-fluorenone imine) results in formation of $[Li(THF)_2]_2[Fe(N{=}C_{13}H_8)_4]$ (**3**), in good yield. Subsequent oxidation of **3** with ca. 0.8 equiv of I_2 generates the $[Fe_2]^{6+}$ complex, $[Fe_2(\mu\text{-}N{=}C_{13}H_8)_2(N{=}C_{13}H_8)_4]$ (**4**), along with free fluorenyl ketazine. Complexes **1**, **2**, and **4** were characterized by ^{1}H NMR spectroscopy, X-ray crystallography, ^{57}Fe Mössbauer spectroscopy, and SQUID magnetometry. The Fe–Fe distances in **1**, **2**, and **4** range from 2.803(7) to 2.925(1) Å, indicating that no direct Fe–Fe interaction is present in these complexes. The ^{57}Fe Mössbauer spectra for complexes **1**, **2**, and **4** are all consistent with the presence of symmetry-equivalent, high-spin Fe^{3+} centers. Finally, all three complexes exhibit a similar degree of antiferromagnetic coupling between the metal centers (J = -23 to -29 cm^{-1}), as ascertained by SQUID magnetometry.

Introduction

Metal–metal communication can play a key role in the emergence of single-molecule magnetism, which has potential applications in data storage and quantum computing.[1–9] For example, Long and co-workers isolated a series of phosphinimide-bridged $[M_4]^{5+}$ clusters, $[M_4(NP^tBu_3)_4]^+$ (M = Ni, Co) that feature high spin ground states and slow magnetic relaxation. The latter observation was attributed to direct exchange interactions,[10–12] which were thought to be a consequence of the relatively short M–M bonds imposed by the bridging phosphinimide ligand. The pyridin-2-yl-amide class of ligands can also promote strong metal–metal interactions, specifically in extended metal atom chains (EMACs).[13–20] For example, $[Cr_5(tdpa)_4X_2]$ (X = Cl^-, SCN^-; H_2tdpa = N^2,N^6-di(pyridine-2-yl)pyridine-2,6-diamine) exhibits strong antiferromagnetic coupling between metal centers, as well as single-molecule magnet behavior at low temperatures.[21] Metal–metal communication can also influence spin crossover (SCO) behavior in multi-metallic complexes,[22–29] which have potential applications in molecular electronics and sensors.[27,30,31] For example, the pyrazolate-bridged $[Fe_2]^{4+}$-containing polymer, $[\{Fe_2(NCS)_2(\mu\text{-bpypz})_2\}(\mu\text{-4,4′-bipy})]$ (Hbpypz = 3,5-bis(2-pyridyl)-pyrazole) exhibits a sharp SCO transition, due, in part, to the *minimal* magnetic exchange coupling between Fe centers.[32] Importantly, each of these examples relies on the ability of ligands to control the magnetic interactions between metal ions.

The ketimide anion, $[N{=}CR_2]^-$, is another ligand class that is adept at promoting metal–metal interactions,[33–35] as shown by the multimetallic complexes, $[Li(12\text{-crown-}4)_2][M_2(\mu\text{-}N{=}C^tBu_2)_3(N{=}C^tBu_2)_2]$ (M = Mn, Fe, Co), $[Fe_2(\mu\text{-}N{=}C^tBu_2)_2(N{=}C^tBu_2)_3]$, $[Fe_4(\mu\text{-}N{=}CPh_2)_6]$, and $[Fe_4(\mu\text{-Br})_2(\mu\text{-}N{=}C^tBu_2)_4]$.[36–38] In the case of $[Fe_4(\mu\text{-}N{=}CPh_2)_6]$ and $[Fe_4(\mu\text{-Br})_2(\mu\text{-}N{=}C^tBu_2)_4]$, metal–metal communication occurs via direct exchange, which leads to ferromagnetic coupling between metal centers.[37,38] In contrast, for $[Fe_2(\mu\text{-}N{=}C^tBu_2)_2(N{=}C^tBu_2)_3]$, metal–metal communication likely occurs via superexchange, which leads to anti-ferromagnetic coupling.[36] While the ability of the ketimide ligand to mediate metal–metal communication is reasonably well established,[33,36,37] the role that the ketimide substituents play in mediating these interactions is not well understood. In fact, the diversity of known ketimide substituents is relatively low and the most common substituents, by a substantial margin, are Ph and ^{t}Bu.[39–54] In this regard, we recently reported the syntheses of two "tied-back" ketimides, 2-adamantyl ketimide and 9-fluorenyl ketimide, in an effort to increase this substituent diversity.[33] The latter example, with its conjugated π-system, could be especially good at promoting metal–metal communication. Herein, we evaluate the magnetic properties of a series of $[Fe_2]^{6+}$ dimers with varying ketimide substituents, including the fluorenyl substituent, in an effort to tune the magnetic interactions between iron centers.

Results and Discussion

Synthesis. The reaction of $Fe(acac)_3$ with 3 equiv of $Li(N{=}CPh_2)$ in tetrahydrofuran (THF) at room temperature for 20 h resulted in the formation of $[Fe_2(\mu\text{-}N{=}CPh_2)_2(N{=}CPh_2)_4]$ (**1**), which was isolated as black needles in 40% yield after work-up (Scheme 1). Similarly, reaction of $Fe(acac)_3$ with 3 equiv of $Li(N{=}C(^tBu)Ph)$ in diethyl ether (Et_2O) at room temperature for 18 h resulted in the formation of $[Fe_2(\mu\text{-}N{=}C(^tBu)Ph)_2(N{=}C(^tBu)Ph)_4]$ (**2**), which was isolated as a black crystalline material in 35% yield after work-up. Complex **1** is soluble in THF, and somewhat soluble in toluene, benzene, and Et_2O, whereas complex **2** is soluble in THF, Et_2O, benzene, and hexanes. As solids, both **1** and **2** are stable under inert atmosphere at -25 °C for several months; however, they decompose rapidly upon exposure to air in both the solid and solution states.

Scheme 1. Synthesis of Complexes **1** and **2**

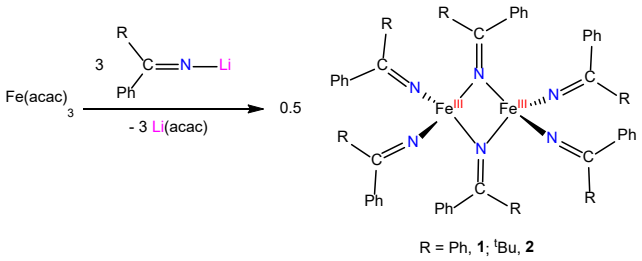

The ^{1}H NMR spectrum of **1** (Figure S5) in C_6D_6 is consistent with the idealized D_{2h} symmetry observed in the solid state (see below). The spectrum exhibits two resonances at 19.52 and 13.49 ppm assignable to the *m*-Ar protons of the terminal and bridging ketimide ligands, respectively, and two resonances at -0.37 and -4.26 ppm assignable to the *p*-Ar protons of the bridging and terminal ketimide ligands. The *o*-Ar proton resonances were not observed, likely due to paramagnetic broadening. The ^{1}H NMR spectrum of **2** in C_6D_6 features seven broad and paramagnetically shifted resonances (Figure S6). There are two resonances in an approximately 18:36 ratio at 19.27 and 16.40 ppm, assignable to the bridging and terminal ^{t}Bu resonances, respectively. An additional three resonances at 18.17, 12.79, and 1.36 ppm, in an approximately 8:8:4 ratio, are assignable to the three expected terminal ketimide aryl resonances, and two resonances at 2.49 and 10.79 ppm are assignable to the *p*-Ar and either the *m*- or *o*-Ar protons of the bridging ketimide ligands. One resonance is not observed, presumably because it is too broad. These assignments are consistent with the idealized C_{2h} symmetry expected for the complex.

In contrast to relatively straight-forward syntheses of **1** and **2** from $Fe(acac)_3$, the reaction of 3 equiv of $Li(N{=}C_{13}H_8)$ ($HN{=}C_{13}H_8$ = 9-fluorenone imine) with $Fe(acac)_3$ results in formation of a complex reaction mixture, according to ^{1}H NMR spectroscopy. However, a two-step synthetic approach involving salt metathesis with Fe^{2+}, followed by oxidation to $[Fe_2]^{6+}$, proved to be successful. In particular, reaction of $FeCl_2$ with 6 equiv of $Li(N{=}C_{13}H_8)$ resulted in formation of $[Li(THF)_2]_2[Fe(N{=}C_{13}H_8)_4]$ (**3**), which was isolated as dark green blocks in 70% yield after work-up (Scheme 2). Complex **3** is soluble in THF and somewhat soluble in Et_2O, but insoluble in hexanes, pentane, and benzene. It is stable under an inert atmosphere at -25 °C for several months. Unfortunately, due to their similar solubilities, we could not completely separate complex **3** from the LiCl by-product. In addition, the highest yields of **3** were achieved when an excess of $Li(N{=}C_{13}H_8)$ was used. If lower amounts of $Li(N{=}C_{13}H_8)$ are employed, then the yields of **3** were reduced and ^{1}H NMR spectra showed the presence of several unidentified Fe-containing products.

The ^{1}H NMR spectrum of **3** in THF-d_8 exhibits four resonances at 31.45, 18.82, 14.27, and 12.52 ppm, in an approximately 1:1:1:1 ratio (Figure S8). The observation of four resonances are consistent with the single ligand environment expected for this complex, while the large chemical shifts are consistent with the anticipated open shell ground state.[55] The ^{7}Li NMR spectrum of **3** exhibits a highly-downfield resonance at 211 ppm, also consistent with a paramagnetic ground state (Figure S9). Additionally, its formulation was confirmed by X-ray crystallography (Figure S3). To our knowledge, **3** is the first fluorenyl ketimide complex to be prepared by salt metathesis. Previously reported fluorenyl ketimide complexes we prepared by disproportionation of 9-diazofluorene or by activation of the N–H bond of 9-fluorenone imine.[56–59]

Given the likely (and potentially variable) presence of LiCl in isolated samples of complex **3**, we performed the oxidation by titration with I_2 in THF, and monitored the conversion to the product by ^{1}H NMR spectroscopy. Formally, this transformation requires two oxidizing equivalents: one to form Fe^{3+} and one to convert the redox-active ketimide ligand to ketazine.[59–61] Typically, the highest yields of **4** were achieved upon addition of ca. 0.8 equiv of I_2 to the reaction mixture (Scheme 2). Consistent with the reaction scheme, ^{1}H NMR spectra of the crude reaction mixtures do contain resonances assignable to free fluorenyl ketazine (Figure S10).[59–61]

Work-up the resulting reaction mixture, followed by storage at -25 °C for 24 h, resulted in the deposition of $[Fe_2(\mu\text{-}N{=}C_{13}H_8)_2(N{=}C_{13}H_8)_4]$ (**4**), as a black crystalline solid in good yields. Separation of any remaining ketazine by-product was achieved by quickly rinsing the isolated material with a small portion of THF. Complex **4** is somewhat soluble in THF, but insoluble in Et_2O, hexanes, pentane, and benzene. Its ^{1}H NMR spectrum in THF-d_8 exhibits four resonances at 15.19, 11.93, 0.15, and -0.39 ppm, which are assignable to the four expected CH environments of the bridging ketimide ligand (Figure S11). Additionally, we observe three resonances at 23.55, 16.04, and -3.67 ppm, which are assignable to three of the terminal ketimide CH resonances. One terminal ketimide CH environment was not observed. Importantly, this spectral signature is consistent with the expected idealized D_{2h} symmetry, and suggests that the bimetallic structure of **4** is maintained in donor solvents. The UV-vis spectrum of **4** is also qualitatively similar to that observed for **1** (Figures S16 and S18), suggesting similar structures in solution. For comparison, oxidation of $[Li(THF)]_2[Fe(N{=}C^tBu_2)_4]$ with 1 equiv of I_2 results in formation of the stable Fe(IV) complex, $[Fe(N{=}C^tBu_2)_4]$,[55] demonstrating the greater redox stability of bis(*tert*-butyl)ketimide vs. fluorenyl ketimide.

Scheme 2. Synthesis of complexes **3** and **4**

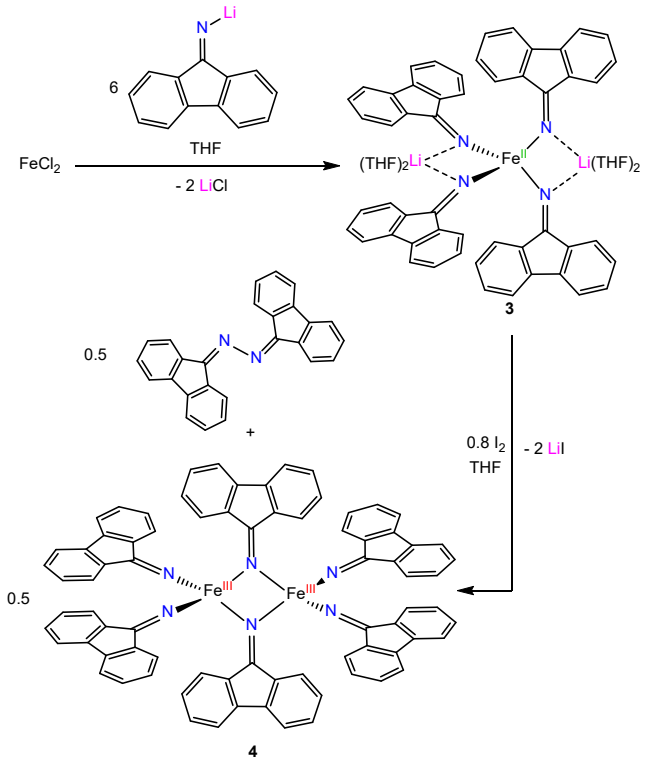

X-ray crystallography. Complexes **1**, **2**, and **4** all crystallize in the triclinic space group *P*-1 (Figures 1, S1, S2, and S4). Complex **1** crystallizes as a toluene solvate, **1**·C_7H_8 with two

independent molecules in the asymmetric unit, whereas **4** crystallizes as a THF solvate, **4**·2THF. All three complexes feature two pseudotetrahedral iron centers bound by two bridging and four terminal ketimide ligands. The Fe–Fe distances are 2.8639(12) and 2.8278(12), 2.9245(13), and 2.803(7) Å for **1**, **2**, and **4**, respectively (Table 1). These values correspond to formal shortness ratios of 1.23 and 1.21, 1.26, and 1.20, respectively,[62,63] and suggest the absence of a direct M–M bonding interaction.[64] For comparison, the imido-bridged $[Fe_2]^{6+}$ complex reported by Holland and co-workers, $[L^{Et}Fe(\mu\text{-}NPh)_2FeL^{Et}]$ (L^{Et} = {(2,6-$Et_2C_6H_3$)NC(Me)}$_2$CH), features a significantly shorter Fe–Fe bond length of 2.5648(4) Å.[65] The Fe–Fe distances in **1**, **2**, and **4** are also much longer than those of the $[Fe_2]^{4+}$ ketimide complex, $[Li(12\text{-crown-}4)_2][Fe_2(\mu\text{-}N{=}C^tBu_2)_3(N{=}C^tBu_2)_2]$ (2.443(1) Å), and the $[Fe_2]^{5+}$ ketimide complex, $[Fe_2(\mu\text{-}N{=}C^tBu_2)_3(N{=}C^tBu_2)_2]$ (2.5468(14) Å).[36] The Fe–Fe distances in **1** are also slightly longer than that of its isostructural $[Fe_2]^{4+}$ congener, $[K(18\text{-crown-}6)]_2[Fe_2(\mu\text{-}N{=}CPh_2)_2(N{=}CPh_2)_4]$ (2.7936(9) Å).[66] As expected, the Fe–$N_{terminal}$ distances are shorter than the Fe–$N_{bridging}$ distances. Finally, the Fe–N–C angles of the terminally-bound ketimide ligands are generally linear, suggesting the presence of π-donation from ketimide to metal (Table 1).

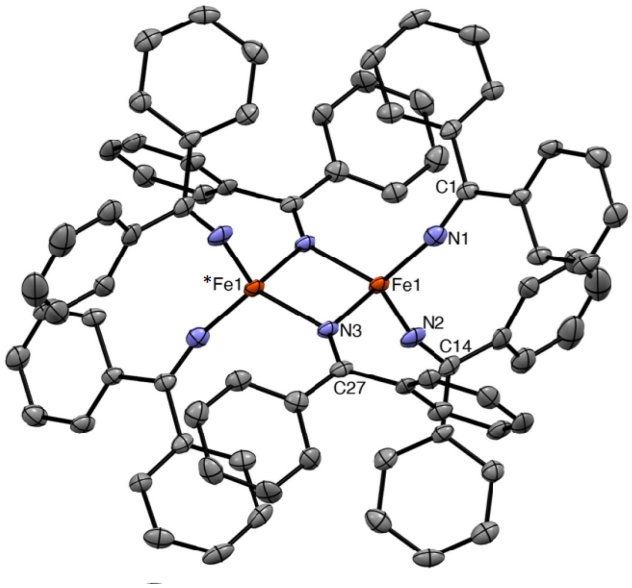

Figure 1. Solid-state molecular structure of **1**·C_7H_8 shown with 50% probability ellipsoids. Hydrogens atoms, second independent molecule, and the toluene solvate have been excluded for clarity.

Table 1. Selected Bond Lengths (Å) and Angles (°) for Complexes **1**, **2**, **4**, and $[K(18\text{-crown-}6)]_2[Fe_2(\mu\text{-}N{=}CPh_2)_2(N{=}CPh_2)_4]$.

Parameter	**1**·C_7H_8	2	**4**·2THF	$[K(18\text{-crown-}6)]_2[Fe_2(N{=}CPh_2)_6]$[66]
Fe–Fe	2.8639(12), 2.8278(12)	2.9245(13)	2.803(7)	2.7936(9)
Formal shortness ratio[62]	1.23, 1.21	1.26	1.20	1.20
Fe–$N_{bridging}$	2.011(3), 2.037(4) 2.001(3), 2.026(3)	2.070(3) 2.085(3)	2.008(8) 2.021(9)	2.045(3) 2.000(3)
Fe–$N_{terminal}$	1.842(4), 1.857(4) 1.848(4), 1.869(3)	1.901(3) 1.927(3)	1.850(9) 1.851(9)	1.941(3) 1.864(3)
Fe–N–$C_{terminal}$	163.6(3), 163.9(3) 171.8(3), 144.6(3)	162.4(3) 167.7(3)	156.1(9) 169.2(9)	171.7(3) 144.3(3)

Mössbauer Spectroscopy and Magnetism. In an effort to confirm their oxidation states, zero-field ^{57}Fe Mössbauer spectroscopy was performed on complexes **1**, **2**, and **4** (Figure 2, Tables 2 and S2). The Mössbauer spectra of all three complexes are very similar. For example, the Mössbauer spectrum of **1** taken at T = 90 K exhibits a sharp asymmetric doublet, with an isomer shift of δ = 0.23 mm/s and quadrupole splitting of $|\Delta E_Q|$ = 0.71 mm/s. The Mössbauer spectrum of **2** features an isomer shift of δ = 0.26 mm/s and quadrupole splitting of $|\Delta E_Q|$ = 0.86 mm/s. Finally, the Mössbauer spectrum of **4** exhibits a sharp asymmetric doublet with an isomer shift of δ = 0.22 mm/s and quadrupole splitting of $|\Delta E_Q|$ = 0.72 mm/s. The presence of a single quadrupole doublet in all three spectra confirm that each complex contains symmetry-related iron environments, consistent with the NMR spectral and X-ray crystallographic data. Moreover, the observed isomer shifts are in line with those expected for high-spin Fe^{3+}.[65,67–72] A comparison with the reported ^{57}Fe Mössbauer parameters for other ketimide-supported clusters and complexes is also informative (Table 2). Generally speaking, there is a good correlation between oxidation state and isomer shift, with one exception. The Fe^{II}/Fe^{I} mixed-valent cluster, $[Fe_4(\mu\text{-}N{=}CPh_2)_6]$, exhibits an anomalously low isomer shift.[37] We do not have a good explanation for this discrepancy at the moment. Also of note, the monometallic Fe^{3+} ketimide, $[Li(12\text{-crown-}4)_2][Fe^{III}(N{=}C^tBu_2)_4]$, features a much larger quadrupole splitting ($|\Delta E_Q|$ = 3.56 mm/s) than those observed for complexes **1**, **2**, or **4**.[73] The large discrepancy is likely a result of the former complex's S = 3/2 spin state, which contrasts to the S = 5/2 spin states of **1**, **2**, and **4** (see below).[74–77]

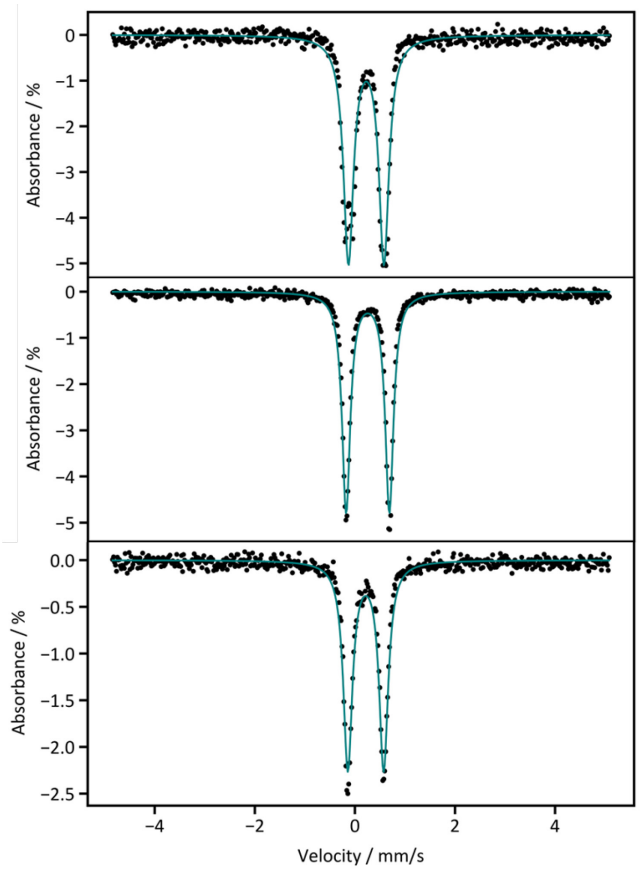

Figure 2. Zero-field ^{57}Fe Mössbauer spectra of **1** (top), **2** (middle), and **4** (bottom) collected at T = 90 K. The teal traces correspond to the overall fit.

Table 2. ^{57}Fe Mössbauer parameters for complexes **1**, **2**, and **4** along with other selected ketimide-supported complexes. O.S. = formal oxidation state.

Complex	δ (mm/s)	$\lvert\Delta E_Q\rvert$ (mm/s)	O.S.	Ref
1	0.23	0.71	3	This work
2	0.26	0.86	3	This work
4	0.22	0.72	3	This work
$[Fe_4(\mu\text{-}N{=}CPh_2)_6]$	0.34	0.79	1.5	[37]
$[Fe_4(\mu\text{-}Br)_2(\mu\text{-}N{=}C^tBu_2)_4]$	0.45	0.62	1.5	[38]
$[Li(THF)]_2[Fe(N{=}C^tBu_2)_4]$	0.44	0.85	2	[73]
$[Li(12\text{-crown-}4)_2][Fe(N{=}C^tBu_2)_4]$	0.19	3.56	3	[73]
$Fe(N{=}C^tBu_2)_4$	-0.15	1.62	4	[73]

Temperature-dependent dc magnetization data were also collected for crystalline samples of **1**, **2**, and **4** at H = 1,000 Oe (Figure 3). Complex **1** exhibits a magnetic moment of $\chi_M T$ = 3.36 emuK mol^{-1} at T = 300 K (μ_{eff} = 5.18 μ_B), which drops precipitously to $\chi_M T$ = 0.003 emuK mol^{-1} at T = 2 K (μ_{eff} = 0.17 μ_B). Likewise, complex **2** exhibits a room-temperature moment of $\chi_M T$ = 3.24 emuK mol^{-1} (μ_{eff} = 5.09 μ_B), which drops to $\chi_M T$ = 0.023 emuK mol^{-1} at T = 2 K (μ_{eff} = 0.43 μ_B). Complex **4** features a higher room-temperature moment of $\chi_M T$ = 4.13 emuK mol^{-1} (μ_{eff} = 5.75 μ_B) that similarly drops to $\chi_M T$ = 0.101 emuK mol^{-1} at T = 2 K (μ_{eff} = 0.90 μ_B). To fit the magnetic data, the exchange Hamiltonian $\widehat{\boldsymbol{H}} = -2\boldsymbol{J}\widehat{\boldsymbol{S}}_{\boldsymbol{Fe}} \cdot \widehat{\boldsymbol{S}}_{\boldsymbol{Fe}}$ was employed. During the fitting process, J and % paramagnetic impurity (S = 5/2) were allowed to refine freely for all three complexes, while the Weiss constant (Θ) was allowed to refine for **4**. The g values were kept constant at $g_1 = g_2$ = 2.00 for **1** and **2**, and $g_1 = g_2$ = 2.10 for **4**, following past precedent.[78–81] D and χ_{TIP} were not included in the fits. Reasonable fits were obtained by assuming $S_1 = S_2$ = 5/2 (Table 3, Figure 3), although the fit for **4** shows small deviations at low and high temperatures (Figure 3 inset). The fits gave magnetic coupling constants of J = -29.0, -29.6, and -25.7 cm^{-1} for complexes **1**, **2**, and **4**, respectively, confirming the strong antiferromagnetic coupling between the Fe^{3+} centers in all three dimers. The magnetic communication in **1**, **2**, and **4** is likely facilitated through superexchange; however, based on the similar J coupling values uncovered for all three complexes, it is clear that the ketimide substituents have a minimal effect on the magnetic communication between metal centers.

Table 3. Hamiltonian parameters from fits to magnetic susceptibility data.

Complex	1	2	4
J (cm^{-1})	-29.0	-29.6	-25.7
g_1, g_2	2.00[a]	2.00[a]	2.10[a]
Paramagnetic Impurity[b] (%)	2.1	1.2	2.4
Θ (K)	--	--	-6.9

[a]Fixed

[b]S = 5/2

For comparison, the magnetic coupling constants in **1**, **2**, and **4** are much smaller than those measured for other ketimide-bridged dimers, such as $[Fe_2(\mu\text{-}N{=}C^tBu_2)_2(N{=}C^tBu_2)_3]$ (J = -235 cm^{-1}), $[Mn_2(\mu\text{-}N{=}C^tBu_2)_3(N{=}C^tBu_2)_2]^-$ (J = -78 cm^{-1}), and $[Li][Cr_2(\mu\text{-}N{=}C_{10}H_{14})_3(N{=}C_{10}H_{14})_4]$ (J = -200 cm^{-1}).[33,36] In the case of the $[Fe_2]^{5+}$ complex, $[Fe_2(\mu\text{-}N{=}C^tBu_2)_2(N{=}C^tBu_2)_3]$, the shorter Fe–Fe distance (2.547(1) Å) likely contributes to the larger coupling.[82,83] Similarly, the $[Fe_2]^{4+}$ complex, $[(PhCN)_2(Mes)_2Fe_2(\mu\text{-}N{=}C(Mes)(Ph))_2]$,[84] also features larger antiferromagnetic coupling (J = -63.7 cm^{-1}) than **1**, **2**, and **4**, likely for the same reason. Several chalcogenide-bridged $[Fe_2]^{6+}$ complexes have also been characterized by magnetometry.[81,85] These exhibit antiferromagnetic coupling constants ranging

from J = -75 cm^{-1} (for [{Fe(salen)}$_2$S]) to -105 cm^{-1} (for [{Fe(bipy)$_2$}$_2$O]$^{4+}$).[85–88] The μ-imido complex, [L^{Et}Fe(μ-NPh)$_2$FeL^{Et}], also features a large antiferromagnetic coupling constant (J = -123 cm^{-1}).[65] In these cases, the superexchange is facilitated by the dianionic bridging ligands, which results in stronger magnetic coupling presumably due to the shorter Fe–$E_{bridging}$ bond lengths. In contrast, [Fe$_2$]$^{6+}$ complexes bridged by monoanionic ligands tend to feature weaker antiferromagnetic couplings,[89] ranging from J = -2.2 cm^{-1} for [Fe$_2$(bbpnol)$_2$] (H$_3$bbpnol = *N*,*N*'-bis(2-hydroxybenzyl)-2-ol-1,3-propanediamine) to J = -28.6 cm^{-1} for [Fe$_2$(chp)$_4$(OMe)$_2$(dmbipy)$_2$] (chp = 6-chloro-2-pyridone; dmbipy = 4,4'-dimethyl-2,2'-bipyridine).[89 90] In this regard, the antiferromagnetic coupling constants measured for **1**, **2**, and **4** are on the upper end of these values, demonstrating that, for monoanionic bridging ligands, ketimides can mediate amongst the strongest metal–metal communication.

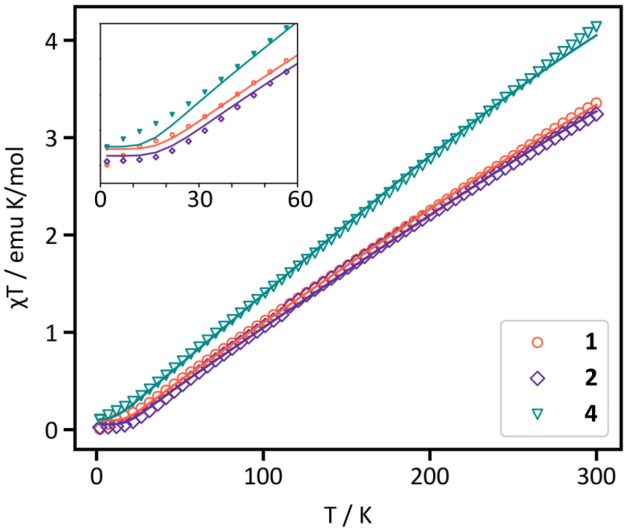

Figure 3. Solid-state magnetic susceptibility data (χ_MT vs. T) for 1 (orange circles), 2 (purple diamonds), and 4 (green triangles) collected under an applied magnetic field of H = 1 kOe from T = 2 to T = 300 K. The solid lines represent fits to the data, as described in the main text. Inset: Expansion of χ_MT vs. T, showing the low temperature data only.

Conclusions

We have synthesized three ketimide-bridged [Fe$_2$]$^{6+}$ complexes with varying substituents on the ketimide ligands. The Fe–Fe bond lengths are similar across the three complexes and do not indicate the presence of direct Fe–Fe interactions. Nonetheless, all three complexes exhibit robust antiferromagnetic communication between Fe centers, likely via superexchange. Surprisingly, however, there is minimal correlation between the substituent identity and the antiferromagnetic exchange coupling constant, even in the case of the fully-conjugated fluorenyl substituent. Despite the lack of any apparent correlation, this work nicely demonstrates the ability of ketimide ligands to generate multi-metallic metal complexes and to facilitate communication between metal centers.

ASSOCIATED CONTENT

Supporting Information

The Supporting Information is available free of charge on the ACS Publications website.

Experimental procedures and crystallographic, spectroscopic, and magnetic characterization details for **1**, **2**, **3**, and **4**. (PDF)

AUTHOR INFORMATION

Corresponding Author

*To whom correspondence should be addressed. Email: hayton@chem.ucsb.edu

Author Contributions

All authors have given approval to the final version of the manuscript.

ACKNOWLEDGMENT

We thank the National Science Foundation (Grant CHE 2055063) for financial support of this work. This research made use of a 400 MHz NMR spectrometer supported in part by the NIH Shared Instrumentation Grant, S10OD012077. The MRL Shared Experimental Facilities are supported by the MRSEC Program of the National Science Foundation under award NSF DMR 1720256, a member of the NSF-funded Materials Research Facilities Network.

REFERENCES

(1) Zabala-Lekuona, A.; Seco, J. M.; Colacio, E. Single-Molecule Magnets: From Mn12-Ac to Dysprosium Metallocenes, a Travel in Time. *Coord. Chem. Rev.* **2021**, *441*, 213984.

(2) Moneo-Corcuera, A.; Nieto-Castro, D.; Cirera, J.; Gómez, V.; Sanjosé-Orduna, J.; Casadevall, C.; Molnár, G.; Bousseksou, A.; Parella, T.; Martínez-Agudo, J. M.; Lloret-Fillol, J.; Pérez-Temprano, M. H.; Ruiz, E.; Galán-Mascarós, J. R. Molecular Memory near Room Temperature in an Iron Polyanionic Complex. *Chem* **2022**, *9*, 377–393.

(3) Wang, H. S.; Zhang, K.; Song, Y.; Pan, Z. Q. Recent Advances in 3d-4f Magnetic Complexes with Several Types of Non-Carboxylate Organic Ligands. *Inorganica Chim. Acta* **2021**, *521*, 120318.

(4) Sánchez, R. H.; Betley, T. A. Thermally Persistent High-Spin Ground States in Octahedral Iron Clusters. *J. Am. Chem. Soc.* **2018**, *140*, 16792–16806.

(5) Nehrkorn, J.; Greer, S. M.; Malbrecht, B. J.; Anderton, K. J.; Aliabadi, A.; Krzystek, J.; Schnegg, A.; Holldack, K.; Herrmann, C.; Betley, T. A.; Stoll, S.; Hill, S. Spectroscopic Investigation of a Metal-Metal-Bonded Fe$_6$ Single-Molecule Magnet with an Isolated S = 19/2 Giant-Spin Ground State. *Inorg. Chem.* **2021**, *60*, 4610–4622.

(6) Toniolo, D.; Scopelliti, R.; Zivkovic, I.; Mazzanti, M. Assembly of High-Spin [Fe$_3$] Clusters by Ligand-Based Multielectron Reduction. *J. Am. Chem. Soc.* **2020**, *142*, 7301–7305.

(7) Greer, S. M.; Gramigna, K. M.; Thomas, C. M.; Stoian, S. A.; Hill, S. Insights into Molecular Magnetism in Metal-Metal Bonded Systems as Revealed by a Spectroscopic and Computational Analysis of Diiron Complexes. *Inorg. Chem.* **2020**, *59*, 18141–18155.

(8) Hernández Sánchez, R.; Zheng, S. L.; Betley, T. A. Ligand Field Strength Mediates Electron Delocalization in Octahedral [(^{H}L)$_2$Fe$_6$(L')$_m$]$^{N+}$ Clusters. *J. Am. Chem. Soc.* **2015**, *137*, 11126–11143.

(9) Cornia, A.; Mannini, M.; Sainctavit, P.; Sessoli, R. Chemical Strategies and Characterization Tools for the Organization of Single Molecule Magnets on Surfaces. *Chem. Soc. Rev.* **2011**, *40*, 3076–3091.

(10) Chakarawet, K.; Atanasov, M.; Marbey, J.; Bunting, P. C.; Neese, F.; Hill, S.; Long, J. R. Strong Electronic and Magnetic Coupling in M$_4$ (M = Ni, Cu) Clusters via Direct Orbital Interactions between Low-Coordinate Metal Centers. *J. Am. Chem. Soc.* **2020**,

142, 19161–19169.

(11) Chakarawet, K.; Bunting, P. C.; Long, J. R. Large Anisotropy Barrier in a Tetranuclear Single-Molecule Magnet Featuring Low-Coordinate Cobalt Centers. *J. Am. Chem. Soc.* **2018**, *140*, 2058–2061.

(12) Leiszner, S. S.; Chakarawet, K.; Long, J. R.; Nishibori, E.; Sugimoto, K.; Platts, J. A.; Overgaard, J. Electron Density Analysis of Metal-Metal Bonding in a Ni_4 Cluster Featuring Ferromagnetic Exchange. *Inorg. Chem.* **2023**, *62*, 192–200.

(13) Cotton, F. A.; Daniels, L. M.; Jordan IV, G. T.; Murillo, C. A. Symmetrical and Unsymmetrical Compounds Having a Linear Co_3^{6+} Chain Ligated by a Spiral Set of Dipyridyl Anions. *J. Am. Chem. Soc.* **1997**, *119*, 10377–10381.

(14) Chipman, J. A.; Berry, J. F. Paramagnetic Metal-Metal Bonded Heterometallic Complexes. *Chem. Rev.* **2020**, *120*, 2409–2447.

(15) Srinivasan, A.; Musgrave, R. A.; Rouzières, M.; Cléac, R.; Mcgrady, J. E.; Hillard, E. A. A Linear Metal-Metal Bonded Tri-Iron Single-Molecule Magnet. *Chem. Commun.* **2021**, *57*, 13357–13360.

(16) Berry, J. F.; Cotton, F. A.; Fewox, C. S.; Lu, T.; Murillo, C. A.; Wang, X. Extended Metal Atom Chains (EMACs) of Five Chromium or Cobalt Atoms: Symmetrical or Unsymmetrical? *Dalt. Trans.* **2004**, *108*, 2297–2302.

(17) Yin, C.; Huang, G.-C.; Kuo, C.-K.; Fu, M.-D.; Lu, H.-C.; Ke, J.-H.; Shih, K.-N.; Huang, Y.-L.; Lee, G.-H.; Yeh, C.-Y.; Chen, C.-H.; Peng, S.-M. Extended Metal-Atom Chains with an Inert Second Row Transition Metal: [Ru5(M5-Tpda)4X2] (Tpda2-) Tripyridyldiamido Dianion, X = Cl and NCS). *J. Amer. Chem. Soc* **2008**, *130*, 10090–10092.

(18) Nicolini, A.; Galavotti, R.; Barra, A. L.; Borsari, M.; Caleffi, M.; Luo, G.; Novitchi, G.; Park, K.; Ranieri, A.; Rigamonti, L.; Roncaglia, F.; Train, C.; Cornia, A. Filling the Gap in Extended Metal Atom Chains: Ferromagnetic Interactions in a Tetrairon(II) String Supported by Oligo-α-Pyridylamido Ligands. *Inorg. Chem.* **2018**, *57*, 5438–5448.

(19) Nicolini, A.; Affronte, M.; SantaLucia, D. J.; Borsari, M.; Cahier, B.; Caleffi, M.; Ranieri, A.; Berry, J. F.; Cornia, A. Tetrairon(II) Extended Metal Atom Chains as Single-Molecule Magnets. *Dalt. Trans.* **2021**, *50*, 7571–7589.

(20) Cotton, F. A.; Murillo, C. A.; Wang, X. Trinuclear Complexes of Copper, Cobalt and Iron with *N,N′*-Di(2-Pyridyl) Formamidinate Ligands, $[M_3(DPyF)_4][PF_6]_2$. *Inorg. Chem. Commun.* **1998**, *1*, 281–283.

(21) Cornia, A.; Barra, A. L.; Bulicanu, V.; Clérac, R.; Cortijo, M.; Hillard, E. A.; Galavotti, R.; Lunghi, A.; Nicolini, A.; Rouzières, M.; Sorace, L.; Totti, F. The Origin of Magnetic Anisotropy and Single-Molecule Magnet Behavior in Chromium(II)-Based Extended Metal Atom Chains. *Inorg. Chem.* **2020**, *59*, 1763–1777.

(22) Turov, Y.; Berry, J. F. Synthesis, Characterization and Thermal Properties of Trimetallic N_3–CrCr···M–N_3 Azide Complexes with M = Cr, Mn, Fe, and Co. *Dalt. Trans.* **2012**, *41*, 8153–8161.

(23) Velazquez-Garcia, J. de J.; Basuroy, K.; Storozhuk, D.; Wong, J.; Demeshko, S.; Meyer, F.; Henning, R.; Techert, S. Metal-to-Metal Communication during the Spin State Transition of a [2 × 2] Fe(II) Metallogrid at Equilibrium and out-of-Equilibrium Conditions. *Dalt. Trans.* **2022**, *51*, 6036–6045.

(24) Nippe, M.; Victor, E.; Berry, J. F. Do Metal–Metal Multiply-Bonded "Ligands" Have a Trans Influence? Structural and Magnetic Comparisons of Heterometallic Cr□Cr···Co and Mo□Mo···Co Interactions. *Eur. J. Inorg. Chem.* **2008**, *2008*, 5569–5572.

(25) Lovell, T.; Stranger, R.; McGrady, J. E. Mutual Interdependence of Spin Crossover and Metal-Metal Bond Formation in $M_2Cl_9^{3-}$ (M = Fe, Ru, Os). *Inorg. Chem.* **2001**, *40*, 39–43.

(26) Murray, K. S.; Kepert, C. J. Cooperativity in Spin Crossover Systems: Memory, Magnetism and Microporosity. *Top Curr Chem* **2012**, *233*, 195–228.

(27) Brooker, S.; Kitchen, J. A. Nano-Magnetic Materials: Spin Crossover Compounds vs. Single Molecule Magnets vs. Single Chain Magnets. *Dalt. Trans.* **2009**, No. 36, 7331–7340.

(28) Brooker, S.; Plieger, P. G.; Moubaraki, B.; Murray, K. S. $[Co^{II}_2L(NCS)_2(SCN)2]$: The First Cobalt Complex to Exhibit Both Exchange Coupling and Spin Crossover Effects. *Angew. Chem. Int. Ed* **1999**, *38*, 408–410.

(29) Schneider, B.; Demeshko, S.; Dechert, S.; Meyer, F. A Double-Switching Multistable Fe_4 Grid Complex with Stepwise Spin-Crossover and Redox Transitions. *Angew. Chemie Int. Ed.* **2010**, *49*, 9274–9277.

(30) Candini, A.; Klyatskaya, S.; Ruben, M.; Wernsdorfer, W.; Affronte, M. Graphene Spintronic Devices with Molecular Nanomagnets. *Nano Lett.* **2011**, *11*, 2634–2639.

(31) Senthil Kumar, K.; Ruben, M. Emerging Trends in Spin Crossover (SCO) Based Functional Materials and Devices. *Coord. Chem. Rev.* **2017**, *346*, 176–205.

(32) Yoneda, K.; Adachi, K.; Hayami, S.; Maeda, Y.; Katada, M.; Fuyuhiro, A.; Kawata, S.; Kaizaki, S. A Steep One-Step [HS–HS] to [LS–LS] Spin Transition in a 4,4′-Bipyridine Linked One-Dimensional Coordination Polymer Constructed from a Pyrazolato Bridged Fe(II) Dimer. *Chem. Commun.* **2006**, No. 1, 45–47.

(33) Kent, G. T.; Cook, A. W.; Damon, P. L.; Lewis, R. A.; Wu, G.; Hayton, T. W. Synthesis and Characterization of Two "Tied-Back" Lithium Ketimides and Isolation of a Ketimide-Bridged [Cr2]6+ Dimer with Strong Antiferromagnetic Coupling. *Inorg. Chem.* **2021**, *60*, 4996–5004.

(34) Soriaga, R. A. D.; Javed, S.; Hoffman, D. M. Synthesis of Copper(I) Complexes with Ketimide and Hydrazide Ligands. *J. Clust. Sci.* **2010**, *21*, 567–575.

(35) Cook, A. W.; Hrobárik, P. H.; Damon, P. L.; Wu, G.; Hayton, T. W. A Ketimide-Stabilized Palladium Nanocluster with a Hexagonal Aromatic Pd7 Core. *Inorg. Chem* **2020**, *59*, 1471–1480.

(36) Lewis, R. A.; Morochnik, S.; Chapovetsky, A.; Wu, G.; Hayton, T. W. Synthesis and Characterization of $[M_2(N{=}C^tBu_2)_5]^-$ (M=Mn, Fe, Co): Metal Ketimide Complexes with Strong Metal-Metal Interactions. *Angew. Chemie - Int. Ed.* **2012**, *51*, 12772–12775.

(37) Cook, A. W.; Bocarsly, J. D.; Lewis, R. A.; Touchton, A. J.; Morochnik, S.; Hayton, T. W. An Iron Ketimide Single-Molecule Magnet $[Fe_4(N{=}CPh_2)_6]$ with Suppressed through-Barrier Relaxation. *Chem. Sci.* **2020**, *11*, 4753–4757.

(38) Hertler, P. R.; Kautzsch, L.; Touchton, A. J.; Wu, G.; Hayton, T. W. Metal-Metal-Bonded Fe_4 Clusters with Slow Magnetic Relaxation. *Inorg. Chem.* **2022**, *61*, 9997–10005.

(39) Nomura, K.; Yamada, J.; Wang, W.; Liu, J. Effect of Ketimide Ligand for Ethylene Polymerization and Ethylene/Norbornene Copolymerization Catalyzed by (Cyclopentadienyl)(Ketimide)Titanium Complexes–MAO Catalyst Systems: Structural Analysis for $Cp^*TiCl_2(NCPh_2)$. *J. Organomet. Chem.* **2007**, *692*, 4675–4682.

(40) Zhang, W.; Nomura, K. Synthesis of (1-Adamantylimido)Vanadium(V) Complexes Containing Aryloxo, Ketimide Ligands: Effect of Ligand Substituents in Olefin Insertion/Metathesis Polymerization. *Inorg. Chem.* **2008**, *47*, 6482–6492.

(41) Assefa, M. K.; Sergentu, D. C.; Seaman, L. A.; Wu, G.; Autschbach, J.; Hayton, T. W. Synthesis, Characterization, and Electrochemistry of the Homoleptic f Element Ketimide Complexes $[Li]_2[M(N{=}C^tBuPh)_6]$ (M = Ce, Th). *Inorg. Chem.* **2019**, *58*, 12654–12661.

(42) Seaman, L. A.; Wu, G.; Edelstein, N.; Lukens, W. W.; Magnani, N.; Hayton, T. W. Probing the 5f Orbital Contribution to the Bonding in a U(V) Ketimide Complex. *J. Am. Chem. Soc.* **2012**, *134*, 4931–4940.

(43) Henderson, K. W.; Hind, A.; Kennedy, A. R.; McKeown, A. E.; Mulvey, R. E. Synthesis of Zirconocene Amides and Ketimides and an Investigation into Their Ethylene Polymerization Activity. *J. Organomet. Chem.* **2002**, *656*, 63–70.

(44) Lukens, W. W.; Edelstein, N. M.; Magnani, N.; Hayton, T. W.; Fortier, S.; Seaman, L. A. Quantifying the σ and π Interactions between U(V) f Orbitals and Halide, Alkyl, Alkoxide, Amide and Ketimide Ligands. *J. Am. Chem. Soc.* **2013**, *135*, 10742–10754.

(45) Shimbayashi, T.; Okamoto, K.; Ohe, K. Generation of Stable Ruthenium(IV) Ketimido Complexes by Oxidative Addition of Oxime Esters to Ruthenium(II): Reactivity Studies Based on Electronic Properties of the Ru−N Bond. *Chem. – A Eur. J.* **2017**, *23*, 16892–16897.

(46) Barr, D.; Clegg, W.; Mulvey, R. E.; Snaith, R.; Wade, K. Bonding Implications of Interatomic Distances and Ligand Orientations in

the Iminolithium Hexamers $[LiNC(Ph)Bu^t]_6$ and $[LiNC(Ph)NMe_2]_6$: A Stacked-Ring Approach to These and Related Oligomeric Organolithium System. *J. Chem. Soc. Chem. Commun.* **1986**, No. 4, 295–297.

(47) Werner, H.; Knaup, W.; Dziallas, M. A Novel Route to Azaalkenylidene-Metal Complexes. *Angew. Chemie Int. Ed. English* **1987**, *26*, 248–250.

(48) Jantunen, K. C.; Burns, C. J.; Castro-Rodriguez, I.; Da Re, R. E.; Golden, J. T.; Morris, D. E.; Scott, B. L.; Taw, F. L.; Kiplinger, J. L. Thorium(IV) and Uranium(IV) Ketimide Complexes Prepared by Nitrile Insertion into Actinide-Alkyl and -Aryl Bonds. *Organometallics* **2004**, *23*, 4682–4692.

(49) Alcock, N. W.; Pierce-Butler, M. Crystal and Molecular Structures of the Tetrakis(Diphenylketimine) Derivatives of Silicon, Germanium, and Tin. *J. Chem. Soc. Dalt. Trans.* **1975**, No. 22, 2469–2476.

(50) Hoberg, H.; Götz, V.; Goddard, R.; Krüger, C. Nickel(O)-Komplexe Mit Benzophenonimin-Lithium Und Benzophenonimin. *J. Organomet. Chem.* **1980**, *190*, 315–324.

(51) Bryan, S. J.; Clegg, W.; Snaith, R.; Wade, K.; Wong, E. H. Structure and Bonding of the Tris(Diphenylmethyleneamino)Aluminium Dimer $[Al(NCPh_2)_3]_2$: Relative Strengths of Bridging and Terminal Al–X Bonds in Systems $X_2Al(\mu_2\text{-}X)_2AlX_2$. *J. Chem. Soc. Chem. Commun.* **1987**, *1*, 1223–1224.

(52) Erker, G.; Frömberg, W.; Krüger, C.; Raabe, E. $Cp_2Zr(N{=}CPh_2)_2$, an Organometallic Heteroallene-Type Schiff Base Derivative Relevant to Describing Sp^2-Hybridized Nitrogen Inversion. *J. Am. Chem. Soc.* **1988**, *110*, 2400–2405.

(53) Edwards, A. J.; Paver, M. A.; Raithby, P. R.; Russell, C. A.; Wright, D. S. Synthesis and Crystal Structure of $Sb(NCPh_2)_3$. *J. Chem. Soc. Dalt. Trans.* **1993**, No. 14, 2257–2258.

(54) Lefeber, C.; Arndt, P.; Tillack, A.; Baumann, W.; Kempe, R.; Burlakov, V. V.; Rosenthal, U. Reactions of the Schiff Bases $HN{=}CPh_2$ and PhN=CHPh with Titanocene- and Zirconocene-Generating Complexes. *Organometallics* **1995**, *14*, 3090–3093.

(55) Lewis, R. A.; Wu, G.; Hayton, T. W. Synthesis and Characterization of an Iron(IV) Ketimide Complex. *J. Am. Chem. Soc.* **2010**, *132*, 12814–12816.

(56) Ren, W.; Zhou, E.; Fang, B.; Hou, G.; Zi, G.; Fang, D. C.; Walter, M. D. Experimental and Computational Studies on the Reactivity of a Terminal Thorium Imidometallocene towards Organic Azides and Diazoalkanes. *Angew. Chemie - Int. Ed.* **2014**, *53*, 11310–11314.

(57) Fang, B.; Zhang, L.; Hou, G.; Zi, G.; Fang, D. C.; Walter, M. D. Experimental and Computational Studies on an Actinide Metallacyclocumulene Complex. *Organometallics* **2015**, *34*, 5669–5681.

(58) Marquard, S. L.; Bezpalko, M. W.; Foxman, B. M.; Thomas, C. M. Interaction and Activation of Carbon-Heteroatom π Bonds with a Zr/Co Heterobimetallic Complex. *Organometallics* **2014**, *33*, 2071–2079.

(59) Zhou, J.; Liu, L. L.; Cao, L. L.; Stephan, D. W. Reductive Coupling and Loss of N_2 from Magnesium Diazomethane Derivatives. *Chem. – A Eur. J.* **2018**, *24*, 8589–8595.

(60) Pfeiffer, J.; Nieger, M.; Dötz, K. H. Chromium Complex Catalyzed Synthesis of Spirocyclopropanes from Diaryl Diazo Compounds-Direct NMR-Spectroscopic Observation of a Carbene Complex Intermediate. *European J. Org. Chem.* **1998**, *1998*, 1011–1022.

(61) Lasri, J.; Eltayeb, N. E.; Ismail, A. I. Experimental and Theoretical Study of Crystal and Molecular Structure of 1,2-Di(9*H*-Fluoren-9-Ylidene)Hydrazine. *J. Mol. Struct.* **2016**, *1121*, 35–45.

(62) Eisenhart, R. J.; Rudd, P. A.; Planas, N.; Boyce, D. W.; Carlson, R. K.; Tolman, W. B.; Bill, E.; Gagliardi, L.; Lu, C. C. Pushing the Limits of Delta Bonding in Metal-Chromium Complexes with Redox Changes and Metal Swapping. *Inorg. Chem.* **2015**, *54*, 7579–7592.

(63) Pauling, L. Atomic Radii and Interatomic Distances in Metals. *J. Am. Chem. Soc.* **1947**, *69*, 542–553.

(64) Duncan Lyngdoh, R. H.; Schaefer, H. F.; King, R. B. Metal-Metal (MM) Bond Distances and Bond Orders in Binuclear Metal Complexes of the First Row Transition Metals Titanium through Zinc. *Chem. Rev.* **2018**, *118*, 11626–11706.

(65) Bellows, S. M.; Arnet, N. A.; Gurubasavaraj, P. M.; Brennessel, W. W.; Bill, E.; Cundari, T. R.; Holland, P. L. The Mechanism of N-N Double Bond Cleavage by an Iron(II) Hydride Complex. *J. Am. Chem. Soc.* **2016**, *138*, 12112–12123.

(66) Sieg, G.; Pessemesse, Q.; Reith, S.; Yelin, S.; Limberg, C.; Munz, D.; Werncke, C. G. Cobalt and Iron Stabilized Ketyl, Ketiminyl and Aldiminyl Radical Anions. *Chem. – A Eur. J.* **2021**, *27*, 16760–16767.

(67) Lee, J. L.; Biswas, S.; Sun, C.; Ziller, J. W.; Hendrich, M. P.; Borovik, A. S. Bioinspired Di-Fe Complexes: Correlating Structure and Proton Transfer over Four Oxidation States. *J. Am. Chem. Soc.* **2022**, *144*, 4559–4571.

(68) Mossin, S.; Tran, B. L.; Adhikari, D.; Pink, M.; Heinemann, F. W.; Sutter, J.; Szilagyi, R. K.; Meyer, K.; Mindiola, D. J. A Mononuclear Fe(III) Single Molecule Magnet with a 3/2↔5/2 Spin Crossover. *J. Am. Chem. Soc.* **2012**, *134*, 13651–13661.

(69) Auerbach, H.; Giammanco, G. E.; Schünemann, V.; Ostrowski, A. D.; Carrano, C. J. Mössbauer Spectroscopic Characterization of Iron(III)-Polysaccharide Coordination Complexes: Photochemistry, Biological, and Photoresponsive Materials Implications. *Inorg. Chem.* **2017**, *56*, 11524–11531.

(70) Bennett, M. V.; Stoian, S.; Bominaar, E. L.; Münck, E.; Holm, R. H. Initial Members of the Family of Molecular Mid-Valent High-Nuclearity Iron Nitrides: $[Fe_4N_2X_{10}]^{4-}$ and $[Fe_{10}N_8X_{12}]^{5-}$ ($X = Cl^-$, Br^-). *J. Am. Chem. Soc.* **2005**, *127*, 12378–12386.

(71) Rodriguez, M. M.; Bill, E.; Brennessel, W. W.; Holland, P. L. N2 Reduction and Hydrogenation to Ammonia by a Molecular Iron-Potassium Complex. *Science* **2011**, *334*, 780–783.

(72) Grubel, K.; Brennessel, W. W.; Mercado, B. Q.; Holland, P. L. Alkali Metal Control over N−N Cleavage in Iron Complexes. *J. Am. Chem. Soc* **2014**, *136*, 16807–16816.

(73) Lewis, R. A.; Smiles, D. E.; Darmon, J. M.; Stieber, S. C. E.; Wu, G.; Hayton, T. W. Reactivity and Mössbauer Spectroscopic Characterization of an Fe(IV) Ketimide Complex and Reivestigation of an Fe(IV) Norbornyl Complex. *Inorg. Chem* **2013**, *52*, 8218–8227.

(74) Schünemann, V.; Winkler, H. Structure and Dynamics of Biomolecules Studied by Mössbauer Spectroscopy. *Reports Prog. Phys.* **2000**, *63*, 263–353.

(75) Kojima, T.; Ogishima, F.; Nishibu, T.; Kotani, H.; Ishizuka, T.; Okajima, T.; Nozawa, S.; Shiota, Y.; Yoshizawa, K.; Ohtsu, H.; Kawano, M.; Shiga, T.; Oshio, H. Intermediate-Spin Iron(III) Complexes Having a Redox-Noninnocent Macrocyclic Tetraamido Ligand. *Inorg. Chem.* **2018**, *57*, 9683–9695.

(76) Bartos, M. J.; Kidwell, C.; Kauffmann, K. E.; Gordon-Wylie, S. W.; Collins, T. J.; Clark, G. C.; Münck, E.; Weintraub, S. T. A Stable Aquairon(III) Complex with S = 1: Structure and Spectroscopic Properties. *Angew. Chemie Int. Ed. English* **1995**, *34*, 1216–1219.

(77) Kostka, K. L.; Fox, B. G.; Hendrich, M. P.; Collins, T. J.; Rickard, C. E. F.; Wright, L. J.; Münck, E. High-Valent Transition Metal Chemistry. Mössbauer and EPR Studies of High-Spin (S = 2) Iron(IV) and Intermediate-Spin (S = 3/2) Iron(III) Complexes with a Macrocyclic Tetraamido-N Ligand. *J. Am. Chem. Soc.* **1993**, *115*, 6746–6757.

(78) Murali, M.; Nayak, S.; Costa, J. S.; Ribas, J.; Mutikainen, I.; Turpeinen, U.; Clémancey, M.; Garcia-Serres, R.; Latour, J. M.; Gamez, P.; Blondin, G.; Reedijk, J. Discrete Tetrairon(III) Cluster Exhibiting a Square-Planar $Fe_4(\mu_4\text{-}O)$ Core: Structural and Magnetic Properties. *Inorg. Chem.* **2010**, *49*, 2427–2434.

(79) Lee, K. H. K.; Peralta, J. E.; Abboud, K. A.; Christou, G. Iron(III)-Oxo Cluster Chemistry with Dimethylarsinate Ligands: Structures, Magnetic Properties, and Computational Studies. *Inorg. Chem.* **2020**, *59*, 18090–18101.

(80) Khanra, S.; Konar, S.; Clearfield, A.; Helliwell, M.; Mclnnes, E. J. L.; Tolis, E.; Tuna, F.; Winpenny, R. E. P. Synthesis, Structural and Magnetochemical Studies of Iron Phosphonate Cages Based on $\{Fe_3O\}^{7+}$ Core. *Inorg. Chem.* **2009**, *48*, 5338–5349.

(81) Weihe, H.; Güdel, H. U. Angular and Distance Dependence of the Magnetic Properties of Oxo-Bridged Iron(III) Dimers. *J. Am. Chem. Soc* **1997**, *119*, 6539–6543.

(82) Henning, J. C. M.; Damen, J. P. M. Exchange Interactions within Nearest-Neighbor Cr^{3+} Pairs in Chromium-Doped Spinel $ZnGa_2O_4$. *Phys. Rev. B* **1971**, *3*, 3852–3854.

(83) Gamage, E. H.; Ribeiro, R. A.; Harmer, C. P.; Canfield, P. C.;

Ozarowski, A.; Kovnir, K. Tuning of Cr-Cr Magnetic Exchange through Chalcogenide Linkers in Cr_2 Molecular Dimers. *Inorg. Chem.* **2022**, *61*, 6160–6174.

(84) Alain Klose, B.; Solan, E.; Floriani, C.; Chiesi-Villa, A.; Rizzoli, C.; Re, N. Magnetic Properties Diagnostic for the Existence of Iron(II)-Iron(II) Bonds in Dinuclear Complexes Which Derive from Stepwise Insertion Reactions on Unsupported Iron-Aryl. *J. Am. Chem. Soc* **1994**, *116*, 9123–9135.

(85) Murray, K. S. Binuclear Oxo-Bridged Iron(III) Complexes. *Coord. Chem. Rev.* **1974**, *12*, 1–35.

(86) Lewis, B. J.; Mabbs, F. E.; Richards, A. The Preparation and Magnetic Properties of Some Oxy-Bridged Binuclear Iron(III) Schiff-Base Complexes. *J. Chem. Soc.* **1967**, 1014–1018.

(87) Khedekar, A. V; Lewis, J.; Mabbs, F. E.; Weigold, H. The Composition and Magnetic Properties of Some Iron(III) 1,10-Phen-Anthroline and Bipyridyl Complexes. *Inorg. Phys. Theor.* **1967**, 1561–1564.

(88) Mitchell, P. C. H.; Parker, D. A. A Sulphido-Bridged Iron(III) Schiff's Base Complex. *J. Inorg. Nucl. Chem.* **1973**, *35*, 1385–1390.

(89) Werner, R.; Ostrovsky, S.; Griesar, K.; Haase, W. Magnetostructural Correlations in Exchange Coupled Phenoxo-, Alkoxo-, and Hydroxo-Bridged Dinuclear Iron(III) Compounds. *Inorganica Chim. Acta* **2001**, *326*, 78–88.

(90) Elmali, A.; Elerman, Y.; Svoboda, I.; Fuess, H.; Griesar, K.; Haase, W. Structures and Magnetic Properties of Dinuclear Iron(III) Complexes. *Zeitschrift fur Naturforsch. - Sect. B J. Chem. Sci.* **1994**, *49*, 365–369.

For Table of Contents Only

A series of ketimide-bridged $[Fe_2]^{6+}$ complexes exhibit strong metal–metal communication, likely via superexchange.